ChemComm

Cite this: *Chem. Commun.*, 2012, **48**, 7931–7933

www.rsc.org/chemcomm

COMMUNICATION

Graphene–Ni–α-MnO_2 and –Cu–α-MnO_2 nanowire blends as highly active non-precious metal catalysts for the oxygen reduction reaction†

Timothy N. Lambert,*[a] Danae J. Davis,[a] Wei Lu,[b] Steven J. Limmer,[c] Paul G. Kotula,[d] Alexis Thuli,[a] Madalyn Hungate,[a] Gedeng Ruan,[b] Zhong Jin[b] and James M. Tour*[b]

Received 25th April 2012, Accepted 17th June 2012
DOI: 10.1039/c2cc32971a

Graphene–like carbon–Ni–α-MnO_2 and –Cu–α-MnO_2 blends can serve as effective catalysts for the oxygen reduction reaction with activities comparable to Pt/C.

Platinum (Pt) metal and Pt-based alloys are effective materials for the oxygen reduction reaction (ORR), with excellent activity towards an apparent four-electron ($n = 4$) reduction of O_2.[1] However, Pt^0 is prohibitively expensive, relatively scarce and can suffer from deleterious poisoning reactions, such as when methanol crossover or carbon monoxide poisoning occurs in fuel cells. Manganese oxide (MnO_x) catalysts have received considerable attention due to their low cost, their being relatively environmentally benign, and their high activity for ORR catalysis.[2–4] α-MnO_2 nanowires are among the most active MnO_x for the ORR in alkaline solution.[5] This activity is attributed to the size (nano-sized MnO_2 > micron-sized-MnO_2), morphology (nanowires/spheres > nanoparticles) and phase (α-MnO_2 > β-MnO_2 > γ-MnO_2). In order to meet the demands of high electrochemical activity and high electronic conductivity, MnO_x/carbon blends or composites are needed for actual application in a working cathode.[6,7] Graphene-based carbons have shown considerable promise as catalysts for the ORR,[8–10] and have been examined as metal and ceramic composites including with, but not limited to Pt,[11] Co_3O_4,[12] $MnCo_2O_4$,[13] $CoMn_2O_4$,[14] ZnSe,[15] Mn_3O_4[16] and MnO_2.[7]

Here, we demonstrate that copper (Cu) or nickel (Ni) doping in α-MnO_2 nanowires (hereby termed Cu–α-MnO_2 or Ni–α-MnO_2) significantly increases their performance, and in particular, when combined with a nano-diameter domain-sized graphene-like carbon (GLC) sheets,[17] specific activities and half wave potentials for the Cu–α-MnO_2 or Ni–α-MnO_2/GLC blends are of similar value to the commercial 20% Pt/C benchmark catalyst. Both the materials are prepared by cost effective solution methods and simply blended together to make the composite catalyst.

The synthesis of α-MnO_2 nanowires was performed by modifying a literature hydrothermal reaction between $MnSO_4 \cdot H_2O$ and $KMnO_4$.[5,18] The synthesis of Cu–α-MnO_2 and Ni–α-MnO_2 nanowires was achieved by the addition of $Cu(NO_3)_2 \cdot 3H_2O$ or $Ni(NO_3)_2 \cdot 6H_2O$, as described in the ESI.† Nanowires, as shown in the scanning electron microscopy (SEM) images in Fig. 1a were obtained exclusively as the α-MnO_2 phase (JCPDS file no. 044-0141), as determined from powder X-ray diffraction (PXRD), Fig. 1b and Fig. S1 (ESI†) and selected area electron diffraction patterns (SAED) on bulk and individual nanowires with scanning transmission electron microscopy (STEM) (Fig. S2–5, ESI†). Energy-dispersive X-ray spectroscopy (EDS) spectral imaging also indicated uniform distribution of Cu (~10%) or Ni (~10–12%, relative to Mn) within the nanowire (Fig. S2–5, ESI†).

Surface areas, pore size and pore volume as determined by N_2 adsorption–desorption measurements, were determined to be 73.6 $m^2\ g^{-1}$, 13.4 nm, 0.306 $cm^3\ g^{-1}$ (α-MnO_2), 54.1 $m^2\ g^{-1}$, 10.3 nm, 0.191 $cm^3\ g^{-1}$ (Ni–α-MnO_2) and 43.7 $m^2\ g^{-1}$, 17.3 nm, 0.263 $cm^3\ g^{-1}$ (Cu–α-MnO_2) (Fig. S6, ESI†).

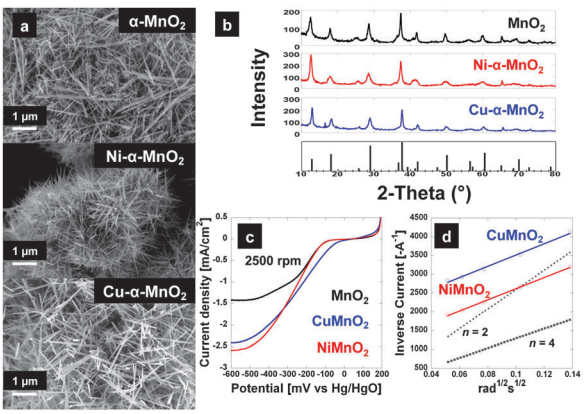

Fig. 1 (a) SEM, (b) PXRD (JCPDS file no. 044-0141), (c) LSVs and (d) Koutecky–Levich plots of nanowires (idealized sloped for $n = 2$ or 4 are also shown).

[a] *Department of Materials, Devices & Energy Technologies, Sandia National Laboratories, Albuquerque, New Mexico, 87185, USA. E-mail: tnlambe@sandia.gov; Fax: 505 844 7786; Tel: 505 284 6967*
[b] *Departments of Chemistry and Mechanical Engineering and Materials Science and the Smalley Institute for Nanoscale Science and Technology, Rice University, Houston, Texas 77005. E-mail: tour@rice.edu; Fax: 713 348 6250; Tel: 713 348 6246*
[c] *Department of Photonic Microsystems Technology, Sandia National Laboratories, Albuquerque, New Mexico, 87185, USA*
[d] *Department of Materials Characterization, Sandia National Laboratories, Albuquerque, New Mexico, 87185, USA*
† Electronic supplementary information (ESI) available: Additional Figures and Experimental Data as noted in the text. See DOI: 10.1039/c2cc32971a

Hence, doping with Ni decreased the surface area, pore size and pore volume, while Cu-doping led to a decrease in surface area and pore volume, but an increase in pore size. These results indicate that the increased activity (*vida infra*) observed with Cu–α-MnO_2 and Ni–α-MnO_2 is not simply a result of an increase in surface area.

As synthesized α-MnO_2, Cu–α-MnO_2 or Ni–α-MnO_2 were drop-coated onto a rotating disk electrode (RDE) from prepared "inks" (ESI†), as RDE studies negate problems of mass-transfer and provides for kinetically controlled processes to be studied.[5] Fig. S7 (ESI†) shows representative linear scanning voltammograms (LSVs) for α-MnO_2, Cu–α-MnO_2 and Ni–α-MnO_2. The increase in current with faster rotation rates is expected, as faster rotation rates correlate with faster O_2 flux to the catalyst surface. Average onset values (*vs.* Hg/HgO) from most negative to least negative were Ni–α-MnO_2 (−112 mV) ≤ α-MnO_2 (−110 mV) <Cu–α-MnO_2 (−75 mV). Fig. 1c compares representative linear scanning voltammograms for the nanowire catalysts at 2500 rpm. Steady state currents (and onsets) for these representative data were −2.59 mA cm^{-2} (−110 mV) for Ni–α-MnO_2 and −2.41 mA cm^{-2} (−70 mV) for Cu–α-MnO_2, as compared to α-MnO_2 at −1.42 mA cm^{-2} (−105 mV). The inclusion of Cu or Ni dopants here provides for improved catalysts with significantly higher steady state currents, with Ni–α-MnO_2 > Cu–α-MnO_2 > α-MnO_2. This is in contrast to similar studies in alkaline electrolyte with Ni-doped α-MnO_2 of nanorod morphology,[19] where Ni-doping only led to a slight increase in steady state currents. The Ni dopant (as prepared here) improves the steady state current with minimal change to the onset while Cu-doping improves the steady state current and demonstrates a slightly earlier onset value than α-MnO_2 and Ni–α-MnO_2.

In order to determine the number of electrons (n) involved in the ORR process, the Koutecky–Levich equation was applied to the data.[20] The obtained plots (i^{-1} *vs.* $\omega^{-1/2}$) for α-MnO_2, Ni–α-MnO_2 and Cu–α-MnO_2 are shown collectively in Fig. 1d and Fig. S8, ESI.† The average n values for α-MnO_2, Cu–α-MnO_2 and Ni–α-MnO_2 were found to be 3.1 ± 0.1, 3.4 ± 0.11 and 3.5 ± 0.05, (from −350 to −600 mV *vs.* Hg/HgO) respectively. Our average obtained value of ~3.1 for α-MnO_2 is consistent with values obtained by others (n = 3.1) under similar RDE conditions.[5] In general, the n values decreased at more negative potentials because the mechanism for the ORR process is sensitive to the applied over-potential.

MnO_x are known to be good catalysts for the decomposition of peroxide while cation doping is known to lower the activation energy for peroxide decomposition.[19,21] Rotating ring disk electrode (RRDE) studies were performed on α-MnO_2, and Ni–α-MnO_2 in order to compare the amount of peroxide produced. Fig. S9 (ESI†) shows that the corrected ring current/disk current produced for both nanowire catalysts is <1%. This remarkably low level of peroxide production across a wide potential range is consistent with a fast peroxide disproportionation reaction in these nanowire structures even without cation doping. Ni-doping in Ni–MnO_x nanoparticles favours the stabilization of Mn(III)/Mn(IV) mediating species involved in the first step of the ORR and may also change the pH dependence on the adsorbed oxygen species.[22] However, more recent work with similar Ni-doped α-MnO_2 nanorods suggests that there are actually fewer of these couples present, but that Ni-doping (~ 9%) induces an increase in exchange current densities.[19] Exchange current densities determined here indicate that Cu-doping and Ni-doping each led to an increase in exchange current density (81.3 μA cm^{-2} and 89.4 μA cm^{-2}, respectively) as compared to α-MnO_2 (65 μA cm^{-2}), indicating that the rate of reaction for ORR is improved with Ni–α-MnO_2 > Cu–α-MnO_2 > α-MnO_2.

Carbon-catalyst blends are required in actual ORR application due to the requirements of high electrochemical activity and high electronic conductivity. Hence, in order to expand the utility of the doped α-MnO_2 nanowires, blended catalyst composites consisting of the catalysts with one of three conductive carbons were examined: commercially available Vulcan carbon (surface area of ~230–250 m^2 g^{-1}), reduced graphene oxide (RGO)[23] (~400–600 m^2 g^{-1}) and a graphene-like carbon (GLC) (~900–1000 m^2 g^{-1}).[17] Vulcan was initially chosen, as it is commercially available and is routinely used in this application, *e.g.* it finds application in our commercial 20% Pt/C benchmark electro-catalyst. In general, higher surface area carbons are often used in an attempt to increase both the specific current density and improve the onset potential of MnO_x nanoparticle/carbon catalyst-composites. We note here that we are examining "blends" of ceramic and carbon prepared using simple mixing protocols, rather than preparing the ceramic *in situ* on the carbon. This approach could be advantageous in screening a variety of graphene-ceramic blends. While we found that Ni–α-MnO_2 catalysts blends using RGO failed to increase catalysis relative to the Ni–α-MnO_2, the catalysts blends with Vulcan and the GLC gave increased performance, Fig. 2a. The GLC blend displays significantly higher steady state currents than the Vulcan blend; however it exhibited a slightly more negative onset potential. Specifically with

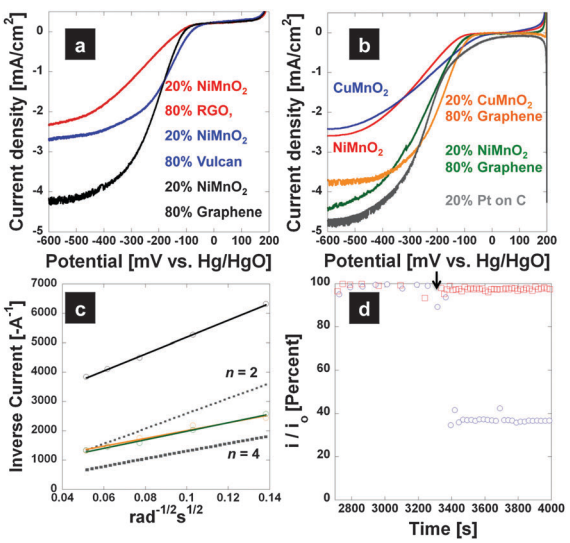

Fig. 2 LSVs of (a) Ni–α-MnO_2/carbon blends, (b) Cu–α-MnO_2, Ni–α-MnO_2 (and GLC blends of) as compared to Pt/C, (c) Koutecky Levich plots for GLC (black circles), 20%Ni–α-MnO_2: 80%GLC (green circles) and 20%Cu–α-MnO_2:80%GLC (orange circles). Idealized slopes for n = 2 or 4 are also shown, (d) Chronoamperometric percent response data for 20%Ni–α-MnO_2:80%GLC (red squares) *versus* Pt/C (blue circles).

Ni–α-MnO_2 blends at −0.6 V (2500 rpm), the Vulcan blend exhibits a steady state current of $-2.6\ \mu A\ cm^{-2}$ with an onset of −84 mV *vs.* Hg/HgO, while the GLC displays $-4.2\ \mu A\ cm^{-2}$ and a −112 mV onset. In general, 20% ceramic/80% GLC provided for the highest steady state currents while higher percentages of ceramic provided for earlier onsets, Fig. S10, ESI.†

Fig. 2b shows LSVs (at 2500 rpm) comparing Ni–α-MnO_2, Cu–α-MnO_2, 20% Ni–α-MnO_2/80% GLC, 20% Cu–α-MnO_2/80% GLC to that of the commercial 20%Pt/C obtained from E-Tek. The combination of the GLC with Ni–α-MnO_2 or Cu–α-MnO_2 provides for a catalyst blend with steady state currents approaching that (91% and 78% respectively, at −0.60 V *vs.* Hg/HgO) of the commercial Pt/C ($-4.6\ \mu A\ cm^{-2}$ and onset of −60 mV *vs.* Hg/HgO) as tested here. Calculated average exchange current densities (and charge transfer resistance values) for the 20% Ni–α-MnO_2/80% GLC were $100.4\ \mu A\ cm^{-2}$ (676 Ω) and 20% Cu–α-MnO_2/80% GLC $97.0\ \mu A\ cm^{-2}$ (594 Ω) are considerably improved relative to Pt/C $47.3\ \mu A\ cm^{-2}$ (1270 Ω). Koutecky–Levich analysis of the linear scanning voltammograms for the GLC tested alone indicates a 2-electron process (average $n = 1.8 \pm 0.03$) for the ORR, Fig. 2c. Koutecky–Levich analysis for the 20% ceramic/80% GLC blends gave slopes approaching that of the idealized $n = 4$ (*e.g.* $n = 3.9 \pm 0.2$ for 20% Cu–α-MnO_2/80% GLC). Additionally, relative kinetic rates of reaction extracted from the Koutecky–Levich data indicate a faster rate of reduction for the GLC blend, with heterogeneous rate constants of, for example, 1.09×10^{-2} cm s^{-1} for 20% Ni–α-MnO_2/80% Vulcan blend *versus* 3.50×10^{-2} cm s^{-1} for the 20% Ni–α-MnO_2/80% GLC blend. The much higher currents obtained with 20% Ni–α-MnO_2/80% GLC *versus* the Vulcan blend are consistent with a higher surface area carbon, Fig. S11 and Table S1, ESI.† For comparison purposes, a value of 3.24×10^{-2} cm s^{-1} was obtained for the 20% Pt/C blend.

RRDE studies demonstrate that GLC produces less peroxide than Vulcan carbon when tested alone, Fig. S12, ESI.† While Pt/C appears to produce less peroxide at higher overpotential, the Cu– and Ni–α-MnO_2:GLC blends exhibit the opposite trend, again consistent with the fact that the mechanism for the ORR process is sensitive to the applied over-potential.

Most important perhaps, is the fact that the half wave potentials for the 20% ceramic/80% GLC blends are very close to that of the 20% Pt/C, Fig. 2b. In fact, between the potential-range from −0.127 V to −0.267 V (*vs.* Hg/HgO), the 20% Cu–α-MnO_2/80% GLC blend outperforms the 20% Pt/C benchmark. The half wave potential region is of particular importance as this is the generally the potential range at which maximum power can be extracted from a fuel cell.[24] With high *n* values, large steady state currents and the fact that the onset and half wave potentials can be further tuned by varying the ratios of GLC:ceramic (Fig. S10, ESI†), these blends hold promise for the development of cathodes for alkaline fuel cells and metal/air batteries.

As an initial probe to examine potential crossover effects in alkaline fuel cells, the electrocatalytic selectivity of 20% Ni–α-MnO_2/80% GLC for ORR *versus* the electro-oxidation of methanol was examined, Fig. 2d and S13 (ESI†).[9,10] Fig. 2d shows the chronoamperometric percent response for the 20% Ni–α-MnO_2/80% GLC blend, as compared to 20% Pt/C. The 20% Pt/C suffers a ∼60% decrease in current upon addition of 2 weight% methanol. In contrast, the 20% Ni–α-MnO_2/80% GLC blend shows a stable amperometric response with less than 5% decrease in current. Hence, the 20% Ni–α-MnO_2/80% graphene-like nanocarbon blend exhibits remarkable tolerance to the crossover effect. In summary, blends of GLC with Ni–α-MnO_2 or Cu–α-MnO_2, prepared by simple mixing protocols, are promising catalysts for the ORR.

This work was supported by: Sandia National Laboratories. Sandia is a multi-program laboratory operated by Sandia Corporation, a Lockheed Martin Company, for the United States Department of Energy's National Nuclear Security Administration under Contract DE-AC04-94AL85000, the AFOSR (FA9550-09-1-0581), and the Office of Naval Research Graphene MURI Program (00006766, N00014-09-1-1066). Ms Bonnie McKenzie and Drs Michael Brumbach and Patrick Burton are thanked for technical assistance.

Notes and references

1 F. Cheng and J. Chen, *Chem. Soc. Rev.*, 2012, **41**, 2172–2192.
2 V. Neburchilov, H. Wang, J. J. Martin and W. Qu, *J. Power Sources*, 2010, **195**, 1271–1291.
3 F. H. B. Lima, M. L. Calegaro and E. A. Ticianelli, *Electrochim. Acta*, 2007, **52**, 3732–3738.
4 E. A. Ticianelli, F. H. B. Lima and M. L. Calegaro, *J. Electroanal. Chem.*, 2006, **590**, 152–160160.
5 F. Cheng, Y. Su, J. Liang, Z. Tao and J. Chen, *Chem. Mater.*, 2010, **22**, 898–905.
6 J.-S. Lee, G. S. Park, H. I. Lee, S. T. Kim, R. Cao, M. Liu and J. Cho, *Nano Lett.*, 2011, **11**, 5362–5366.
7 Y. Qian, S. Lu and F. Gao, *Mater. Lett.*, 2011, **65**, 56–58.
8 J. Xiao, D. Mei, X. Li, W. Xu, D. Wang, G. L. Graff, W. D. Bennett, Z. Nie, L. V. Saraf, I. A. Aksay, J. Liu and J.-G. Zhang, *Nano Lett.*, 2011, **11**, 5071–5078.
9 K. Gong, F. Du, Z. Xia, M. Durstock and L. Dai, *Science*, 2009, **323**, 760–764.
10 L. Qu, Y. Liu, J.-B. Baek and L. Dai, *ACS Nano*, 2010, **4**, 1321–1326.
11 B. Seger and P. V. Kamat, *J. Phys. Chem. C*, 2009, **113**, 7990–7995.
12 Y. Liang, Y. Li, H. Wang, J. Zhou, J. Wang, T. Regier and H. Dai, *Nat. Mater.*, 2011, **10**, 780–786.
13 Y. Liang, H. Wang, J. Zhou, Y. Li, J. Wang, T. Regier and H. Dai, *J. Am. Chem. Soc.*, 2012, **134**, 3517–3523.
14 L. Wang, X. Zhao, Y. Lu, M. Xu, D. Zhang, R. S. Ruoff, K. J. Stevenson and J. B. Goodenough, *J. Electrochem. Soc.*, 2011, **158**, A1379–A1382.
15 P. Chen, T.-Y. Xiao, H.-H. Li, J.-J. Yang, Z. Wang, H.-B. Yao and S.-H. Yu, *ACS Nano*, 2011, **6**, 712–719.
16 J.-S. Lee, T. Lee, H.-K. Song, J. Cho and B.-S. Kim, *Energy Environ. Sci.*, 2011, **4**, 4148–4154.
17 Z. Jin, Z. Sun, L. J. Simpson, K. J. O'Neill, P. A. Parilla, Y. Li, N. P. Stadie, C. C. Ahn, C. Kittrell and J. M. Tour, *J. Am. Chem. Soc.*, 2010, **132**, 15246–15251.
18 F. Y. Cheng, J. Z. Zhao, W. Song, C. S. Li, H. Ma, J. Chen and P. W. Shen, *Inorg. Chem.*, 2006, **45**, 2038–2044.
19 E. M. Benbow, S. P. Kelly, L. Zhao, J. W. Reutenauer and S. L. Suib, *J. Phys. Chem. C*, 2011, **115**, 22009–22017.
20 S. Treimer, A. Tang and D. C. Johnson, *Electroanalysis*, 2002, **14**, 165–171.
21 I. Roche, E. Chaînet, M. Chatenet and J. Vondrák, *J. Appl. Electrochem.*, 2008, **38**, 1195–1201.
22 I. Roche, E. Chaînet, M. Chatenet and J. Vondrák, *J. Phys. Chem. C*, 2007, **111**, 1434–1443.
23 D. C. Marcano, D. V. Kosynkin, J. M. Berlin, A. Sinitskii, Z. Sun, A. Slesarev, L. B. Alemany, W. Lu and J. M. Tour, *ACS Nano*, 2010, **4**, 4806–4814.z
24 R. J. Stanis, T. N. Lambert and M. A. Yaklin, *Energy Fuels*, 2010, **24**, 3125–3129.